

Electronic Supporting Information

Regulating zinc deposition behaviors by using a functional PANI modification layer on a separator for high performance aqueous zinc-ion batteries

Fangfang Wu,^a Fukai Du,^a Pengchao Ruan,^b Gangfeng Cai,^a Ye Chen,^a Xinyu Yin,^a Lu Ma,^a Ruilian Yin,^c Wenhui Shi,^d Wenxian Liu,^a Jiang Zhou,^b and Xiehong Cao^{*a}

^a College of Materials Science and Engineering, Zhejiang University of Technology, 18 Chaowang Road, Hangzhou 310014, P. R. China.

^b College of Materials Science and Engineering, Central South University, 932 South Lushan Road, Changsha 410083, P. R. China.

^c College of Chemical Engineering, Zhejiang University of Technology, 18 Chaowang Road, Hangzhou 310014, Zhejiang, P. R. China

^d Center for Membrane and Water Science & Technology, Zhejiang University of Technology, 18 Chaowang Road, Hangzhou 310014, P. R. China.

* To whom the corresponding should be addressed: gcscaoxh@zjut.edu.cn (Xiehong Cao).

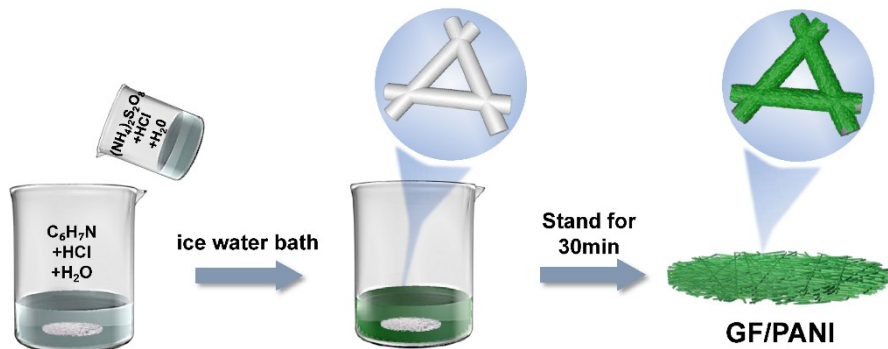


Fig. S1 Schematic illustration of the process of GF/PANI composite separator.



Fig. S2 Digital photographs of the GF/PANI-600 (left) and the pristine GF (right) separator.

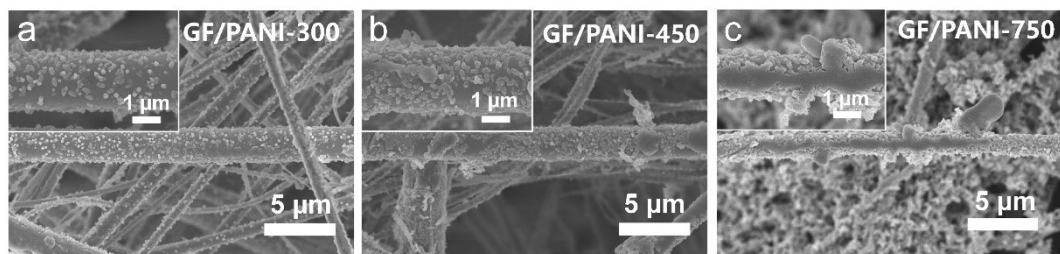


Fig. S3 SEM images of (a) GF/PANI-300, (b) GF/PANI-450 and (c) GF/PANI-750.

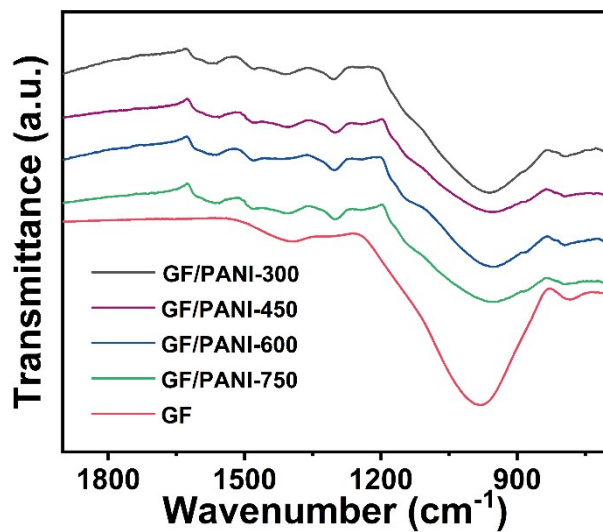


Fig. S4 FTIR of GF separators modified with different volumes of aniline monomers.

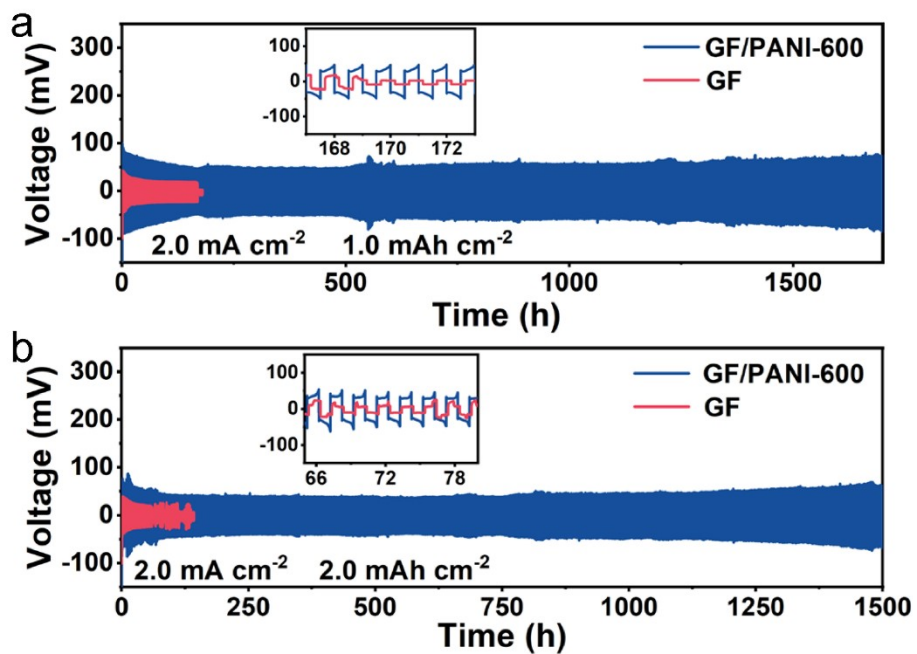


Fig. S5 Cycling stability of $\text{Zn}|\text{GF/PANI-600}|\text{Zn}$ at (a) 2.0 mA cm^{-2} , 1.0 mAh cm^{-2} and (b) 2.0 mA cm^{-2} , 2.0 mAh cm^{-2} .

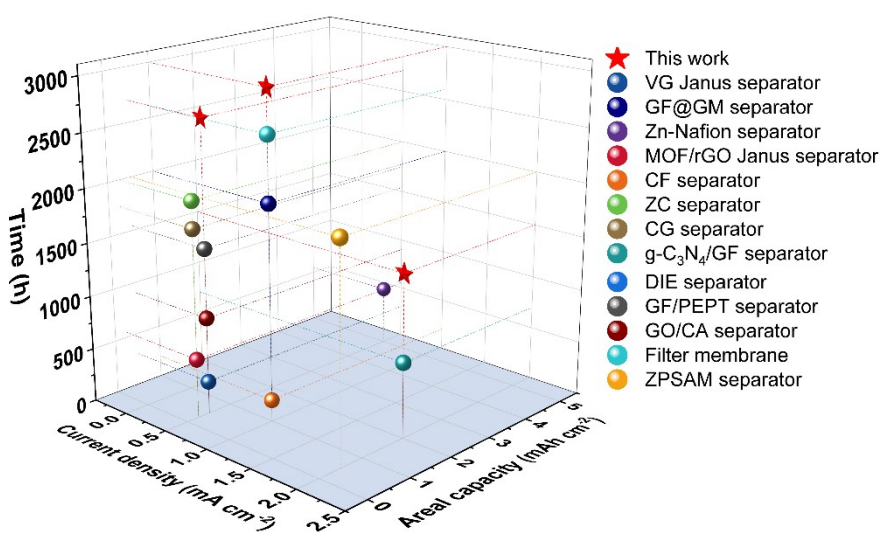


Fig. S6 Comparison of areal capacity, current density, and cycling time with reported separators of AZIBs.

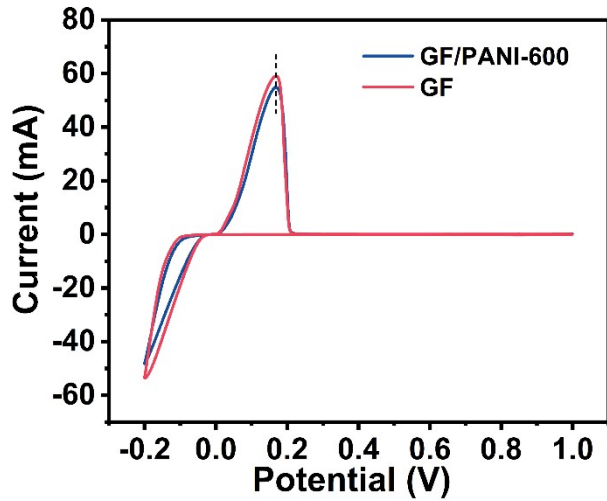


Fig. S7 CV curves of Zn||Cu batteries with GF/PANI-600 and GF separators at scan rate of 1.0 mV s^{-1} .

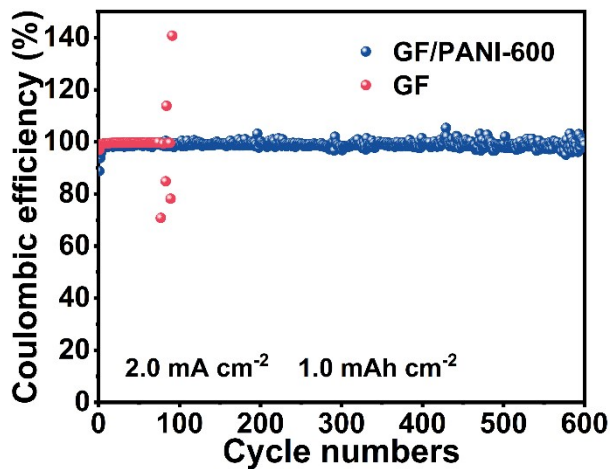


Fig. S8 Coulombic efficiency of Zn||Cu asymmetric batteries with GF/PANI-600 and pristine GF separators at 2.0 mA cm^{-2} , 1.0 mAh cm^{-2} .

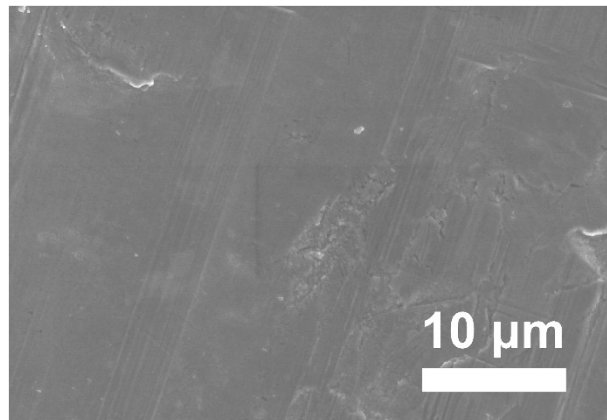


Fig. S9 SEM image of pristine Zn foil.

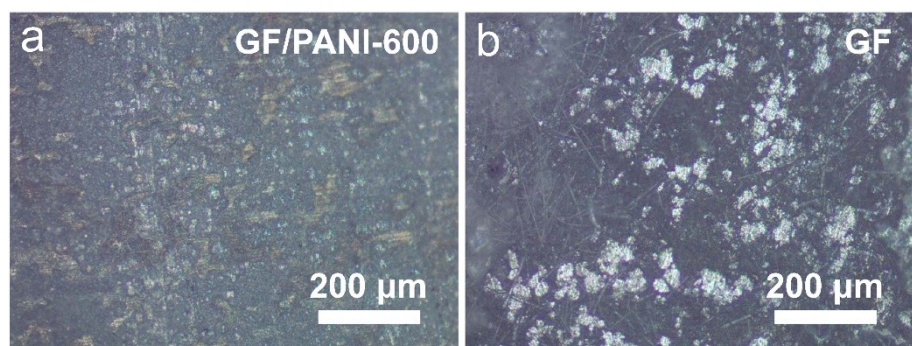


Fig. S10 Optical images of Zn anode at 20 mA cm^{-2} with 4 mAh cm^{-2} after 30 min for $\text{Zn}||\text{Zn}$ battery using (a) GF/PANI-600 and (b) GF separators.

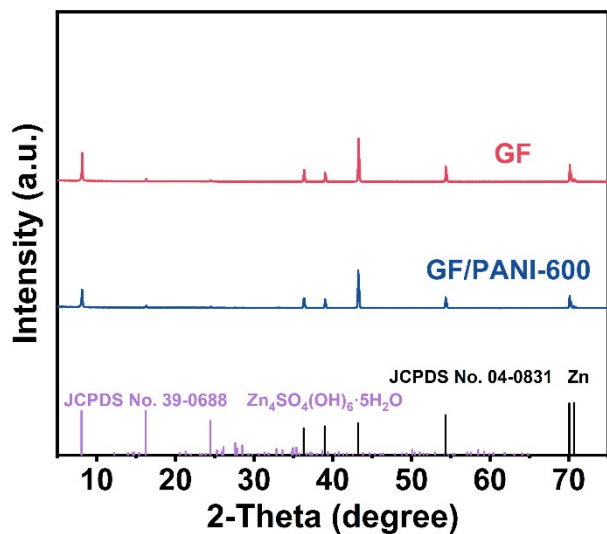


Fig. S11 The XRD of Zn anode for $\text{Zn}||\text{Zn}$ batteries using different separator after 20 cycles at 0.5 mA cm^{-2} , 0.5 mAh cm^{-2} .

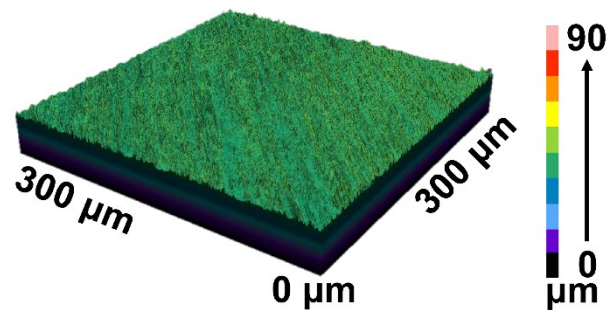


Fig. S12 3D confocal microscopy image of pristine Zn foil.

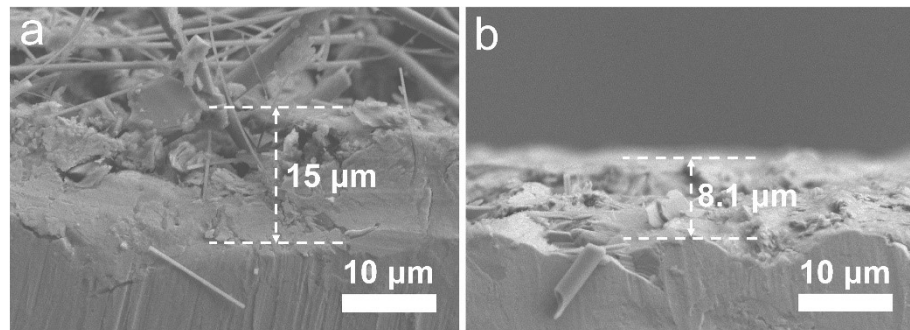


Fig. S13 Cross-sectional SEM image of zinc anode after 20 cycles at 0.5 mA cm^{-2} and 0.5 mAh cm^{-2} (a) GF and (b) using GF/PANI-600 separator.

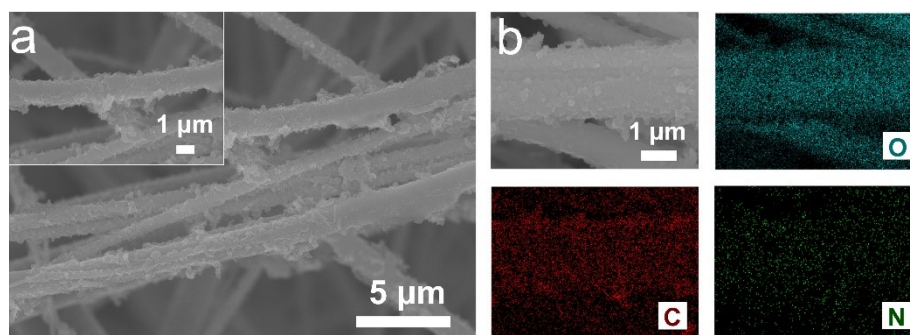


Fig. S14 (a) SEM and (b) elemental mapping images of GF/PANI-600 at 0.5 mA cm^{-2} with 0.5 mAh cm^{-2} after 50 cycles.

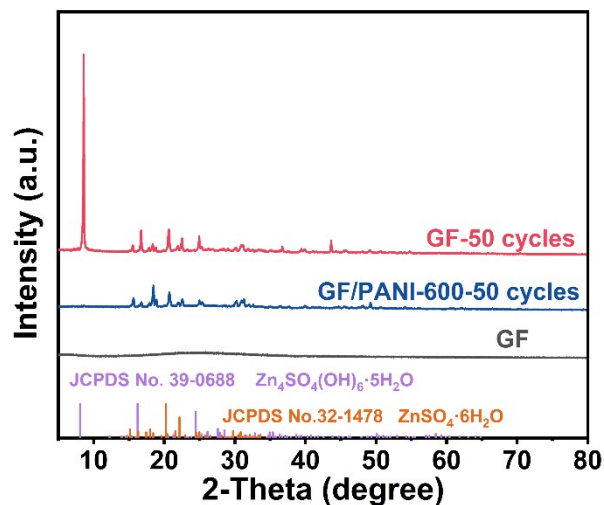


Fig. S15 XRD patterns of GF/PANI-600 and GF separators cycled at 0.5 mA cm^{-2} with 0.5 mAh cm^{-2} after 50 cycles.

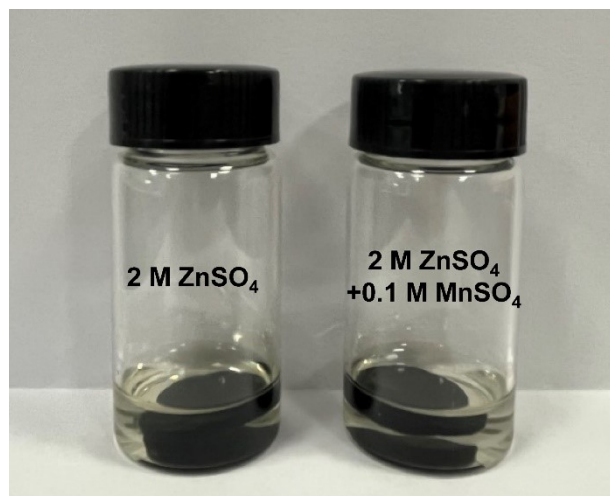


Fig. S16 Digital photographs of GF/PANI-600 soaked in 2 M ZnSO₄ (left) and 2 M ZnSO₄ + 0.1 M MnSO₄ electrolytes (right) for 60 days.

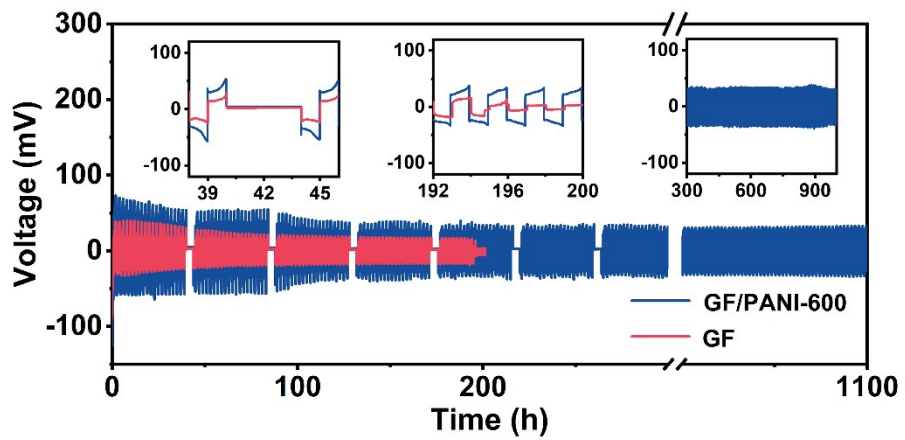


Fig. S17 Cycling and resting process of $\text{Zn}||\text{Zn}$ symmetric batteries with GF and GF/PANI-600 separators at 0.5 mA cm^{-2} , and 0.5 mAh cm^{-2} .

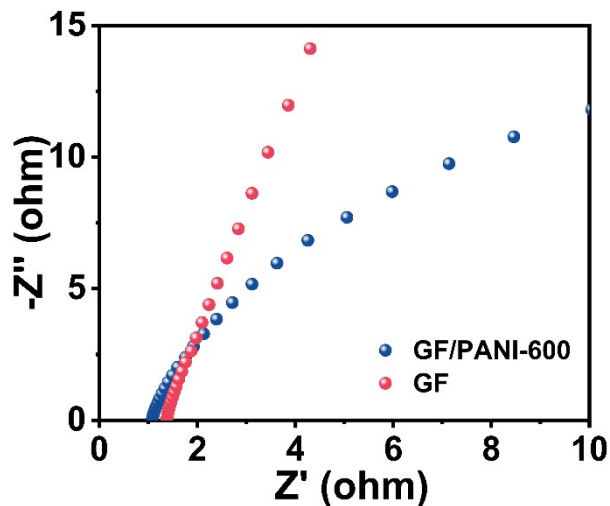


Fig. S18 Nyquist plots of SS|GF/PANI-600|SS and SS|GF|SS batteries.

The ionic conductivity (σ) was measured by EIS tests using stainless steel||stainless steel (SS||SS) symmetric batteries and calculated by the equation:

$$\sigma = \frac{L}{R \times S}$$

where L is the thickness of the separator, S is the contact area between the separator and the stainless steel electrode, and R (Ω) is the bulk resistance acquired from the intercept of Nyquist plots with the real axis. The calculated σ values of GF separator and GF/PANI-600 separator are 2.46×10^{-2} mS cm⁻¹ and 3.25×10^{-2} mS cm⁻¹, respectively.

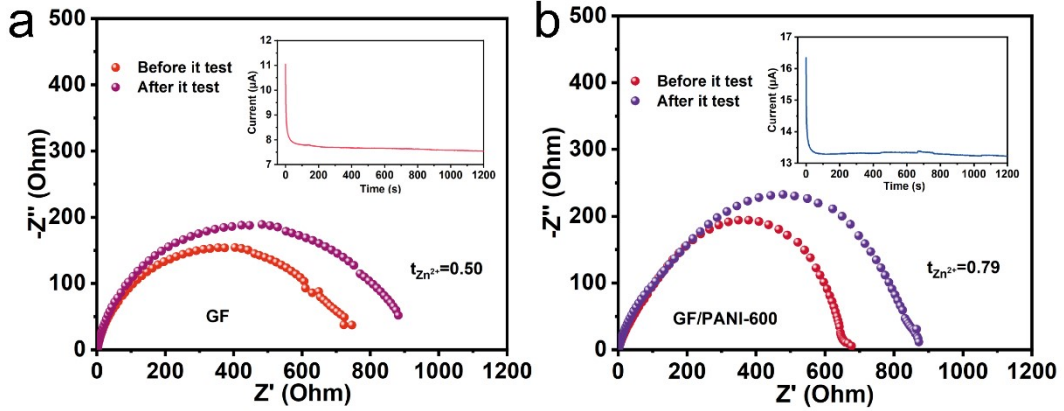


Fig. S19 Nyquist plots of tested batteries before/after polarization at room temperature for Zn||Zn battery (a) GF and (b) GF/PANI-600 separator (insets: Time-dependence response of potentiostatic DC polarization).

The transfer number of Zn^{2+} was calculated based on the following equation:

$$t_{\text{Zn}^{2+}} = \frac{I_s(\Delta V - I_0 R_0)}{I_0(\Delta V - I_s R_s)}$$

where I_0 and I_s are the initial and steady current, ΔV is the applied constant potential across the Zn||Zn symmetric batteries, and R_0 and R_s are the initial and steady current and interfacial resistance. ΔV was set as 10 mV.

The I_0/I_s , and R_0/R_s for GF separator and GF/PANI-600 are 11.05/7.54 μA , 604.40/730.70 Ω and 16.35/13.23 μA , 657.10/813.60 Ω , respectively.

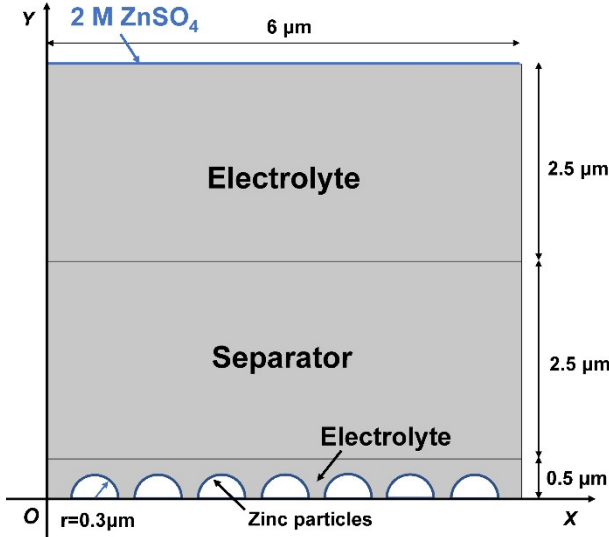


Fig. S20 Simulations domains, dimensions, and boundary conditions used in this study.

The area, size and boundary conditions are constructed by this model and shown in Fig. S20. The model include electrolyte, separator, zinc anode, etc., in which seven semicircles are designed to represent the protrusions of the zinc anode. The ionic transport of the zinc anode was predicted using Nernst-Planck formula:¹

$$\nabla \cdot (-D_i \nabla c_i - z_i \mu_{m,i} F c_i \nabla U) + u \cdot \nabla c_i = R_i$$

$$\nabla \cdot j^U = F \sum_i z_i R_i$$

$$\sum_i z_i c_i = 0$$

$$J_i = -D_i \nabla c_i - z_i \mu_{m,i} F c_i \nabla U + u c_i$$

$$J^U = F \sum_i z_i (-D_i \nabla c_i - z_i \mu_{m,i} F c_i \nabla U)$$

where J_i is the mass flux of each species, D_i is the diffusion coefficient ($3.36 \times 10^{-5} \text{ cm}^2 \text{ s}^{-1}$ for Zn^{2+} and $1.38 \times 10^{-5} \text{ cm}^2 \text{ s}^{-1}$ for SO_4^{2-}), c_i is the concentration, z_i is the charge number (Zn^{2+} is 2 and SO_4^{2-} is -2), ∇U is the electrolyte potential, and F is the Faraday constant. The process does not consider convection, so μ is 0. The boundary condition is to set the experimentally determined polarization voltage of the symmetric battery to the cathode potential and the anode potential to the constant 0.

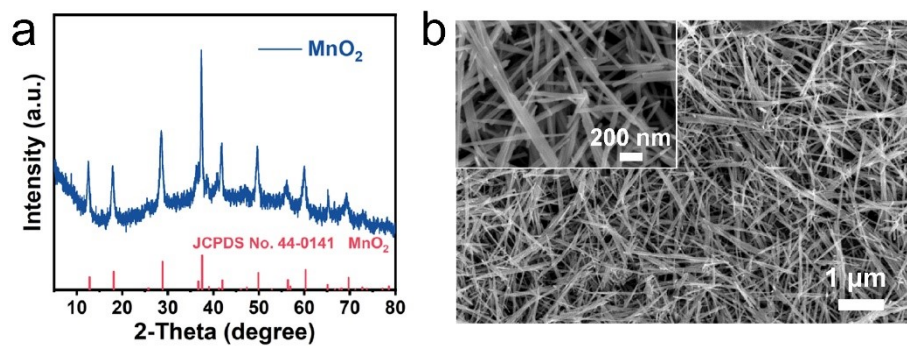


Fig. S21 (a) XRD pattern and (b) SEM image of MnO₂.

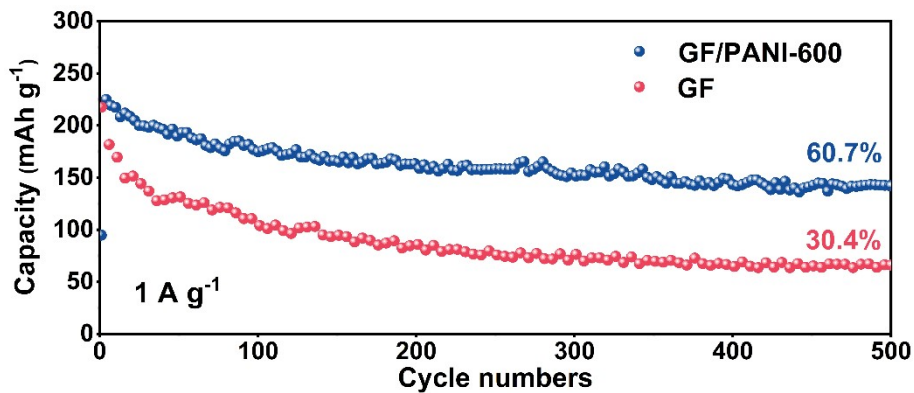


Fig. S22 Cycling performances of Zn||MnO₂ full batteries using GF and GF/PANI-600 separators at 1.0 A g⁻¹.

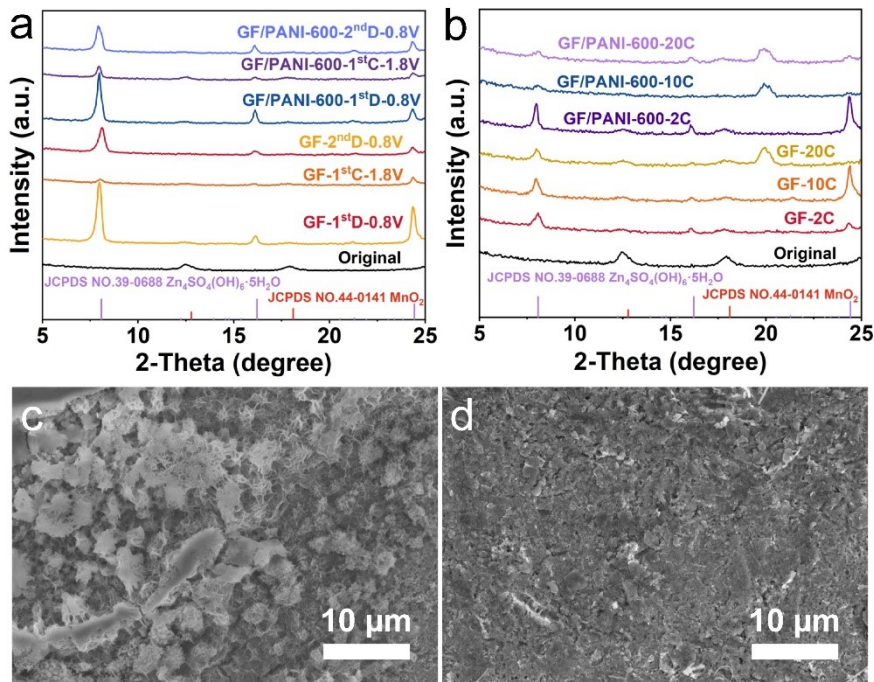


Fig. S23 *Ex-situ* XRD patterns of MnO₂ cathode collected at different states for Zn||MnO₂ batteries with GF and GF/PANI-600 separators at 0.5 A g⁻¹ (a) after different discharge/charge states and (b) after different cycles. SEM images of Zn anodes of Zn||MnO₂ batteries using (c) GF and (d) GF/PANI-600 separators after 20 cycles at 0.5 A g⁻¹.

Table S1. Electrochemical performance comparison of Zn||Zn symmetric batteries using GF/PANI-600 and other reported separators.

Separator	Current density (mA cm ⁻²)	Areal capacity (mAh cm ⁻²)	Time (h)	Reference
GF/PANI-600 separator	1	1	3000	This work
	0.5	0.5	2700	
	2	2	1500	
Vertical graphene modified separator (VG Janus separator)	0.5	0.5	300	2
Separator decorated with functional supramolecules (GF@GM separator)	1	1	2000	3
Zn ²⁺ substituted Nafion separator (Zn-Nafion separator)	0.5	5	553	1
MOF/rGO bifunctional interlayers modified separator (MOF/rGO Janus separator)	0.5	0.25	550	4
Cellulose film separator (CF separator)	1	1	200	5
Cellulose nanofibers-ZrO ₂ composite separator (ZC separator)	0.5	0.25	2000	6
Separator composed of cellulose nanofibers and graphene oxide (CG separator)	0.5	0.25	1750	7
g-C ₃ N ₄ nanosheet-modified GF (g-C ₃ N ₄ /GF separator)	2	2	700	8
Dual-interface engineering modified separator (DIE separator)	10	0.25	1600	9
Incorporating poly (biphenyl piperidinium triphenylmethane) modified separator (GF/PEPT separator)	0.5	0.5	1540	10
Graphene oxide nanosheet-modified cellulose acetate separator (GO/CA separator)	0.5	0.5	900	11
Water-based filter membrane (Filter membrane)	1	1	2600	12
Zincic perfluorinated sul-fonic acid membrane (ZPSAM separator)	2	0.5	2000	13

Table S2. R_{Sz} , R_{Sa} , R_{Sq} values of Zn anode using different separators after different cycles.

	GF -10 cycles	GF -20 cycles	GF -50 cycles	GF/PANI- 600 -10 cycles	GF/PANI- 600 -20 cycles	GF/PANI- 600 -50 cycles
R_{Sz}	45.41	35.63	43.88	13.73	22.52	25.83
R_{Sa}	4.31	5.78	7.37	1.29	1.92	1.959
R_{Sq}	5.96	6.82	8.43	1.70	2.39	2.53

The parameter calculation of surface roughness in Table S2.

Arithmetic average surface roughness (R_{Sa}) represents the arithmetic mean of the deviation of the surface from the reference plane:

$$R_{Sa} = \frac{1}{A} \iint_A |z(x,y)| dx dy$$

Root mean square roughness (R_{Sq}) represents the root mean square value of the ordinate values within the defined area:

$$R_{Sq} = \sqrt{\iint_A |z^2(x,y)| dx dy}$$

Profile micro-roughness (R_{Sz}) means the average value of five randomly selected peak-to-valley distances (N1, N2, N3, N4, N5):

$$R_{Sz} = \frac{N1 + N2 + N3 + N4 + N5}{5}$$

References

1. B. Wu, Y. Wu, Z. Lu, J. Zhang, N. Han, Y. Wang, X.-m. Li, M. Lin and L. Zeng, *J. Mater. Chem. A*, 2021, **9**, 4734-4743.
2. C. Li, Z. Sun, T. Yang, L. Yu, N. Wei, Z. Tian, J. Cai, J. Lv, Y. Shao, M. H. Rummeli, J. Sun and Z. Liu, *Adv. Mater.*, 2020, **32**, 2003425.
3. T. Liu, J. Hong, J. Wang, Y. Xu and Y. Wang, *Energy Storage Mater.*, 2022, **45**, 1074-1083.
4. Z. Wang, L. Dong, W. Huang, H. Jia, Q. Zhao, Y. Wang, B. Fei and F. Pan, *Nano-Micro Lett.*, 2021, **13**, 73.
5. W. Zhou, M. Chen, Q. Tian, J. Chen, X. Xu and C.-P. Wong, *Energy Storage Mater.*, 2022, **44**, 57-65.
6. J. Cao, D. Zhang, C. Gu, X. Zhang, M. Okhawilai, S. Wang, J. Han, J. Qin and Y. Huang, *Nano Energy*, 2021, **89**, 106322.
7. J. Cao, D. Zhang, C. Gu, X. Wang, S. Wang, X. Zhang, J. Qin and Z. S. Wu, *Adv. Energy Mater.*, 2021, **11**, 2101299.
8. L. Wu, Y. Zhang, P. Shang, Y. Dong and Z.-S. Wu, *J. Mater. Chem. A*, 2021, **9**, 27408-27414.
9. Y. Liang, D. Ma, N. Zhao, Y. Wang, M. Yang, J. Ruan, G. Yang, H. Mi, C. He and P. Zhang, *Adv. Funct. Mater.*, 2022, **32**, 2112936.
10. X. Liu, W. Wei, Y. Yang, Y. Li, Y. Li, S. Xu, Y. Dong and R. He, *Chem. Eng. J.*, 2022, **437**, 135409.
11. Y. Luo, Y. Yang, Y. Tao, D. Huang, B. Huang and H. Chen, *ACS Appl. Energy Mater.*, 2021, **4**, 14599-14607.
12. Y. Qin, P. Liu, Q. Zhang, Q. Wang, D. Sun, Y. Tang, Y. Ren and H. Wang, *Small*, 2020, **16**, 2003106.
13. Y. Cui, Q. Zhao, X. Wu, Z. Wang, R. Qin, Y. Wang, M. Liu, Y. Song, G. Qian, Z. Song, L. Yang and F. Pan, *Energy Storage Mater.*, 2020, **27**, 1-8.